ature ozonolysis and UV process. Exposure to an oxygen plasma converts the P(PMDSS) to SiO$_2$ but the directionality of the plasma etch is problematic for the 3D double gyroid structure. A plasma asher that does not contain a forward bias or the use of higher gas pressures in the oxygen reactive ion etcher are ways to reduce the directionality of the plasma process.

15. P(PMDSS) homopolymer was spincast from a 5 wt% solution in toluene onto Si(100) wafers. The solution was directly filtered onto the wafers by using a syringe equipped with a 0.2-μm filter. The samples were then annealed in a vacuum oven at 60°C to drive off excess toluene. The resulting thickness of these samples was 200 nm as measured by profilometry. The samples were then exposed to the same ozone + UV process (see above).
16. J. H. Greiner, *J. Appl. Phys.* **42**, 5151 (1971).
17. The uneven surface prevented the measurement of refractive index or thickness because measured values varied greatly depending on where the measurement was taken.
18. In the current production of high-temperature coatings, silicon-containing homopolymers are pyrolyzed at high temperatures ($T > 600°C$) in order to produce silicon oxycarbide [V. Belot, R. J. P. Corriu, D. Leclercq, P. H. Mutin, A. Vioux, *J. Non-Cryst. Solids* **176**, 33 (1994)]. The oxidized P(PMDSS) homopolymer itself could have utility as high-temperature coatings for materials such as fibers.
19. T. Hashimoto, K. Tsutsumi, Y. Funaki, *Langmuir* **13**, 6869 (1997).
20. J. S. Lee, A. Hirao, S. Nakahama, *Macromolecules* **22**, 2602 (1989).
21. V. Z.-H Chan *et al.*, U.S. and PCT patent PCT/US99/15068.
22. D. J. Kinning, E. L. Thomas, J. M. Ottino, *Macromolecules* **20**, 1129 (1987).
23. www.itrs.net/ntrs/publntrs.nsf
24. J. Joannopoulos, *Photonic Crystals: Molding the Flow of Light* (Princeton Univ. Press, Princeton, NJ, 1995); A. Urbas, Y. Fink, E. L. Thomas, *Macromolecules* **32**, 4748 (1999).
25. We thank R. J. Composto and H. Wang for help with RBS experiments and P. Derege for helpful discussions. The NSF MRSEC shared experimental facilities at MIT were used. Funding was provided by Air Force Office of Scientific Research–ASSERT No. F49 620-94-1-0357, by the NSF Center for Polymer Interfaces and Macromolecular Assemblies (CPIMA) at IBM, and by NSF and IBM through graduate research fellowships for V.Z.-H.C., who also thanks S. Adams for inspiration.

4 August 1999; accepted 19 October 1999

Single-Bond Formation and Characterization with a Scanning Tunneling Microscope

H. J. Lee and W. Ho*

A scanning tunneling microscope (STM) was used to manipulate the bonding of a carbon monoxide (CO) molecule and to analyze the structure and vibrational properties of individual products. Individual iron (Fe) atoms were evaporated and coadsorbed with CO molecules on a silver (110) surface at 13 kelvin. A CO molecule was transferred from the surface to the STM tip and bonded with an Fe atom to form Fe(CO). A second CO molecule was similarly transferred and bonded with Fe(CO) to form Fe(CO)$_2$. Controlled bond formation and characterization at the single-bond level probe chemistry at the spatial limit.

The ability to control chemistry at the spatial limit of individual atoms and molecules provides insights into the nature of the chemical bond and reactivity. As a step toward the realization of this goal, it is necessary to probe the properties of individual molecules and manipulate and alter their chemical composition.

The scanning tunneling microscope (STM) has been used to move and position single atoms (*1*–*3*) and molecules (*4*). The tip of the STM catalyzes surface reactions (*5*). Electrons tunneling through the electronic states of a molecule adsorbed on a surface also couple to intrinsic molecular motions such as rotation (*4*, *6*) and vibration (*7*, *8*), leading to the possibility of inducing chemical transformation in the molecule. Dissociation of single molecules has been accomplished on both metal (*9*) and semiconductor (*10*) surfaces. Although bond cleavage is central in chemical reactions, understanding the reverse process of bond formation, albeit a more difficult one to accomplish experimentally, is equally desirable.

Here, we used a low-temperature STM in an ultrahigh vacuum (*11*) to form a single bond and to characterize the reactants and products with spatial imaging and vibrational spectroscopy. Starting with a clean Ag(110) surface at 13 K, individual Fe atoms were first evaporated onto the surface, and then CO molecules were coadsorbed from the gas phase. We limited exposures of Fe and CO to yield coverages of $\sim$0.001 monolayer to circumvent interactions between coadsorbed species. With the STM, a single CO molecule was bonded to an Fe atom, thus making an Fe(CO) molecule on the surface. A second CO molecule could then be added to form Fe(CO)$_2$. The reactants and products were identified by their distinct STM images and vibrational energies.

The controlled formation of a Fe–CO bond with the STM consisted of a series of systematic steps (Fig. 1). The STM feedback remained on throughout the process. After taking a topographical image of the surface at 70-mV sample bias and 0.1-nA tunneling current, we positioned the tip over a CO molecule (Fig. 1A) adsorbed on top of a Ag

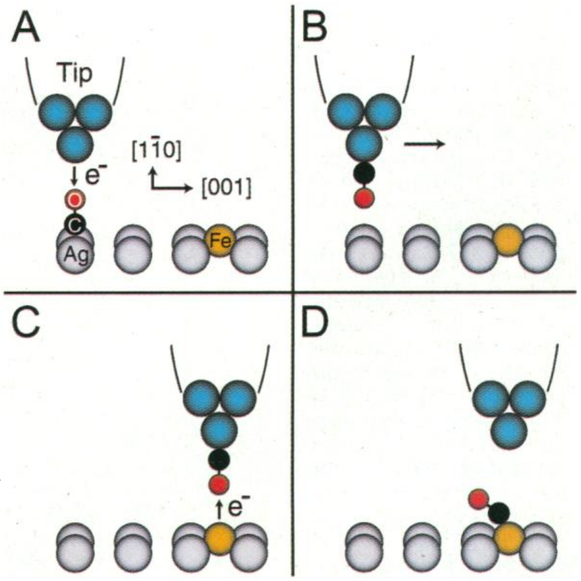

Fig. 1. Schematic diagrams showing the different steps in the formation of a single bond with the STM. The binding sites are determined by imaging the adsorbed species with a CO molecule attached to the tip (Fig. 4). The sizes of the circles are scaled to the atomic covalent radii. The polycrystalline tungsten tip is sputtered and annealed before use; physical contact is made with the Ag surface to further condition the tip. (**A**) The tip is positioned over a single CO molecule to induce the detachment of CO from Ag and its bonding to the tip. Because CO forms a bond predominantly through the carbon, a 180° rotation of the CO occurs in the transfer. (**B**) The tip with the attached single CO molecule is translated (indicted by the arrow) and positioned over an Fe atom. (**C**) The bias voltage and the flow of electrons are reversed, inducing the transfer of CO from the tip to the Fe. (**D**) A single Fe–CO bond is formed. The interaction of the electric field with the dipole moment of CO may also play a role in the transfer of (A) and (C).

Laboratory of Atomic and Solid State Physics and Cornell Center for Materials Research, Cornell University, Ithaca, NY 14853–2501, USA.

*To whom correspondence should be addressed. E-mail: wilsonho@ccmr.cornell.edu

atom (the "atop" site). The bias voltage was then increased to 250 mV, and the tunneling current was ramped from 0.1 to 10 nA to induce the transfer of the CO molecule to the tip (Fig. 1, A and B) (*12*). The bias and tunneling current were then reduced to 70 mV and 0.1 nA, and the tip was translated and positioned over an Fe atom (Fig. 1B) adsorbed on the four-fold hollow site. We formed the Fe–CO bond by first changing the bias to −70 mV, increasing the tunneling current to 10 nA, and finally ramping the bias to about −4 mV (Fig. 1, C and D) (*13*).

The different steps involved in the formation of Fe(CO) and $Fe(CO)_2$ were visualized in a sequence of STM topographical images (Fig. 2). A CO molecule and an Fe atom were selected (Fig. 2A) to form Fe(CO) by the procedure described above (Fig. 2B). The CO ligand in Fe(CO) appears as a side lobe; the asymmetry implies that the CO is not bonded with its axis perpendicular to the surface but is inclined to one side. The Fe(CO) product images as a protrusion of lesser height than a bare Fe atom. The formation of a second neighboring Fe(CO) demonstrates the reproducibility and precision of single-bond formation (Fig. 2C). The addition of a second CO to Fe(CO) yielded a pair of distinct double protrusions for the $Fe(CO)_2$ product (Fig. 2D). The positions of the two protrusions suggest that the two CO ligands are symmetrically located on the Fe atom. A 180° flip was also observed for the remaining Fe(CO) image (Fig. 2, C and D), which suggests a double-well potential with a low energy barrier separating the two equivalent orientations for the CO ligand. Apparently, the two-fold symmetry of the Ag(110) surface makes it less favorable for the CO ligand to occupy the other two orientations 90° away. The STM images also suggest the same constraint in orientation for $Fe(CO)_2$, which exhibits a stable configuration.

Inelastic electron tunneling spectroscopy (IETS) with the STM (*7*, *8*, *11*) provides further identification and insights into the nature of bonding of individual products (Fig. 3). In a topographical image, $^{12}C^{16}O$ and $^{13}C^{18}O$ appear identical. However, by comparing images of the same area after sequential adsorption, the locations of each isotope can be determined, enabling the selective formation of the products $Fe(^{12}C^{16}O)$, $Fe(^{13}C^{18}O)$, $Fe(^{12}C^{16}O)_2$, $Fe(^{13}C^{18}O)_2$, and $Fe(^{12}C^{16}O)(^{13}C^{18}O)$. The Ag(110) spectrum provides a reference for discerning the vibrational peaks (Fig. 3, line A). A single peak is observed at 236 meV (1 meV = 8.065 cm^{-1}) for $Fe(^{12}C^{16}O)$ and is assigned to the C–O stretch (Fig. 3, line B). This peak is downshifted to 224 meV for the $Fe(^{13}C^{18}O)$ isotope (Fig. 3, line C). The corresponding energies of the C–O stretch for $Fe(^{12}C^{16}O)_2$ and $Fe(^{13}C^{18}O)_2$ are 234 and 220 meV, respectively (Fig. 3, lines D and E). Although the C–O stretch peak is revealed in each spectrum, its visibility is enhanced by subtracting the spectra

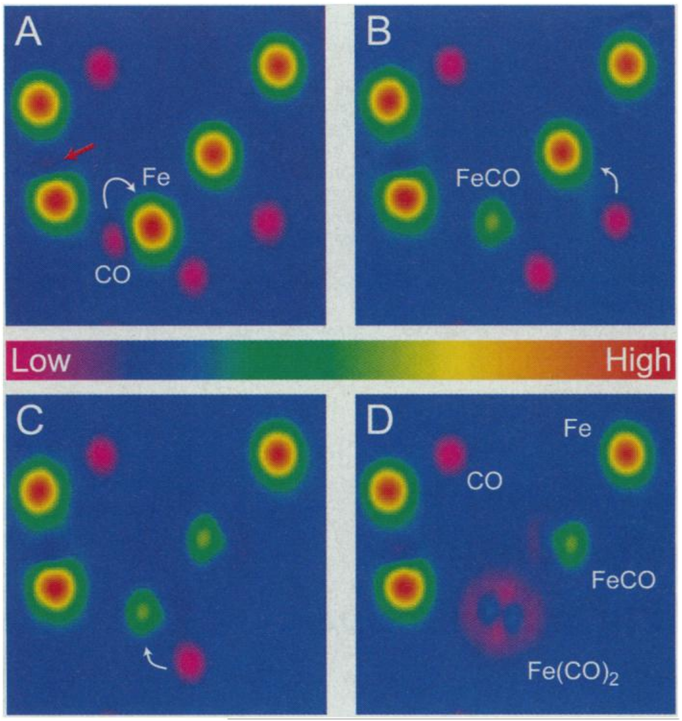

Fig. 2. A sequence of STM topographical images recorded at 70-mV bias, 0.1-nA tunneling current, and 13 K to show the formation of Fe–CO bond with the prescribed method (Fig. 1). The size of each image is 63 Å by 63 Å. Fe atoms image as protrusions and CO molecules as depressions. The white arrows indicate the pair of adsorbed species involved in each bond formation step. (**A**) Five Fe atoms and five CO molecules are adsorbed in this area of the Ag(110) surface. One CO is very close to an Fe atom (indicated by the red arrow). (**B**) A CO molecule has been manipulated and bonded to an Fe atom to form Fe(CO). (**C**) Another Fe(CO) is formed by binding CO to a second Fe atom. (**D**) An additional CO has been bonded to Fe(CO) to form $Fe(CO)_2$. A 180° flip is observed for the remaining Fe(CO).

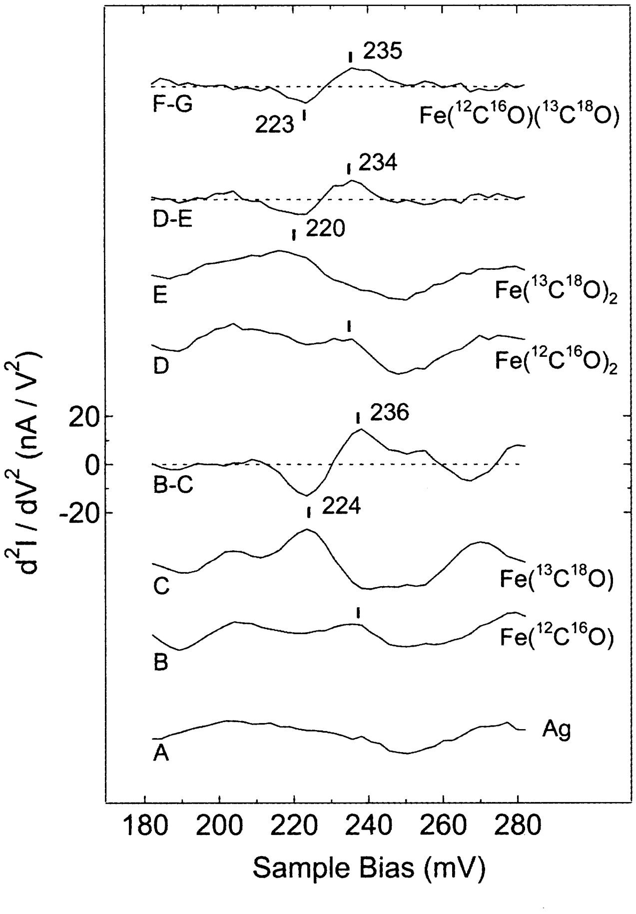

Fig. 3. Single-molecule vibrational spectra obtained by STM-IETS, showing the C–O stretch of Fe(CO) and $Fe(CO)_2$. The differential change of the ac conductance as a function of the sample bias (d^2I/dV^2) is displayed. For each scan, the dc sample bias was ramped from 180 to 280 mV and back down in 2.5-mV steps with a 300-ms dwell time per step (1 meV = 8.065 cm^{-1}). Each spectrum has been signal averaged with repeated scans. The root-mean-square ac modulation at 200 Hz was 7 mV. Peak positions have an uncertainty of ±1 meV. (Line A) Spectrum taken over clean Ag(110) surface and signal averaged with 100 scans. (Line B) Spectrum averaged with 210 scans over the edge of the lobe in the image of single-molecule $Fe(^{12}C^{16}O)$. (Line C) Spectrum averaged with 210 scans over the edge of the lobe in the image of $Fe(^{13}C^{18}O)$. (Line B-C) Difference between spectra B and C. (Line D) Spectrum averaged with 100 scans over the left protrusion in the STM image of the single-molecule $Fe(^{12}C^{16}O)_2$. (Line E) Corresponding spectrum averaged with 100 scans for $Fe(^{13}C^{18}O)_2$. (Line D-E) Difference between spectra D and E. (Line F-G) Difference between spectra recorded separately over the left ($^{12}C^{16}O$, 697 scans) and right ($^{13}C^{18}O$, 280 scans) protrusions in the STM image of the single-molecule $Fe(^{12}C^{16}O)(^{13}C^{18}O)$. Dashed lines denote zero level in difference spectra.

for the isotopes (Fig. 3, lines B-C and D-E), thus emphasizing the vibrational contributions. The electronic contributions to the spectra should be almost identical for the corresponding isotopes. Slight inhomogeneity in the Ag(110) surface may contribute to an incomplete subtraction. For the product with mixed isotopes, Fe($^{12}C^{16}O$)($^{13}C^{18}O$), STM-IETS spectra were recorded separately over the $^{12}C^{16}O$ and $^{13}C^{18}O$ ligands to reveal a C–O stretch at 235 and 223 meV, respectively (Fig. 3, line F-G).

The observed C–O stretch at 236 meV for Fe($^{12}C^{16}O$) is near that of CO adsorbed on the atop site of Fe(100), 234 meV (*14*). For the single-molecule product Fe($^{12}C^{16}O$)$_2$, the observed downshift of the C–O stretch by 2 meV from Fe($^{12}C^{16}O$) can be compared with a downshift of 2.6 meV for Fe(CO)$_2$ in the gas phase (*15*). The observed isotope shift of 12 meV between Fe($^{12}C^{16}O$) and Fe($^{13}C^{18}O$) is in good agreement with the calculated value of 11.5 meV (*16*) and an experimental value of 11.2 meV measured in hemoglobin (*17*). These vibrational analyses provide convincing spectroscopic support for the identification of the single-molecule products as Fe(CO) and Fe(CO)$_2$ (*18*).

The adsorption sites for the reactants and products cannot be determined if the underlying lattice is not resolved in the STM images (Fig. 2). By attaching a CO molecule to the tip (*19*), however, the spatial resolution is substantially increased to allow direct imaging of the Ag atoms, the atop sites for the CO molecules, and four-fold hollow sites for the Fe atoms, Fe(CO), and Fe(CO)$_2$ (Fig. 4E). A stable "supersharp" tip is thereby formed. The STM image for Fe(CO) (Fig. 4C) rules out the geometry with the C–O axis perpendicular to the surface; the side lobe in the image requires a tilt (τ), bend (β), or both (Fig. 4, F and G). An azimuthally symmetric image is expected for a perpendicular geometry (Fig. 4, A and B). Furthermore, spatially resolved vibrational spectra with STM-IETS show the C–O stretch intensity to be localized over the side lobe. The STM image for Fe(CO)$_2$ (Fig. 4D) is also consistent with a tilt (τ'), bend (β'), or both (Fig. 4, H and I). Although our STM images and vibrational spectra indicate an inclined geometry for Fe(CO) and Fe(CO)$_2$, they do not lead to a quantitative determination of the angles, which requires comparison with theoretical calculations.

The adsorption of CO is expected to initiate with the occupation of surface sites that form the strongest bonds. However, this may not always occur in the case in which there is a small number of adsorption sites that form strong bonds and a larger number that form weaker bonds. The bond strengths for gas phase (CO)$_4$Fe–CO, (CO)$_3$Fe–CO, (CO)$_2$Fe–CO, (CO)Fe–CO, and Fe–CO have been determined to be 42 ± 2, 28 ± 9, 29 ± 6, 37 ± 4, and 11 ± 4 kcal/mol, respectively (*20*). The activation energy for desorption of CO from the atop sites of Fe(100) is about 12.8 kcal/mol (*21*). In comparison, the activation energy for desorption of CO from Ag(110) is 5.5 ± 0.4 kcal/mol (*22*). The bond strengths for (CO)Fe–CO and Fe–CO on the Ag(110) surface are expected to be modified from the gas phase values because of the coordination of the Fe to the surface. However, the above energetics and the experimental evidence for a Ag-coated STM tip (*19*) imply that the CO can form stronger bonds with the Fe atoms compared with the Ag surface or the tip. Because CO does not diffuse on Ag(110) at 13 K, formation of Fe(CO) during the adsorption of CO requires a CO molecule to impinge directly on an adsorbed Fe atom. Consequently, for low coverages of Fe and CO, the formation of such Fe(CO) was rare and still rarer for Fe(CO)$_2$ even though it is thermodynamically more favorable for a CO molecule to bind to Fe or Fe(CO) than to the Ag(110) surface. The proximity requirement for the two reactants is further visualized in Fig. 2A, where a CO molecule (indicated by the red arrow) is very close to an Fe atom (~5 Å apart), but no bonding was detected with STM-IETS. In the process of forming Fe(CO) and Fe(CO)$_2$ with the STM, the STM junction can be viewed as a reactor of atomic dimensions in which tunneling electrons and possibly the electric field are involved in overcoming the energetic barriers between the stable bonding sites of CO on the surface, the tip, and the Fe.

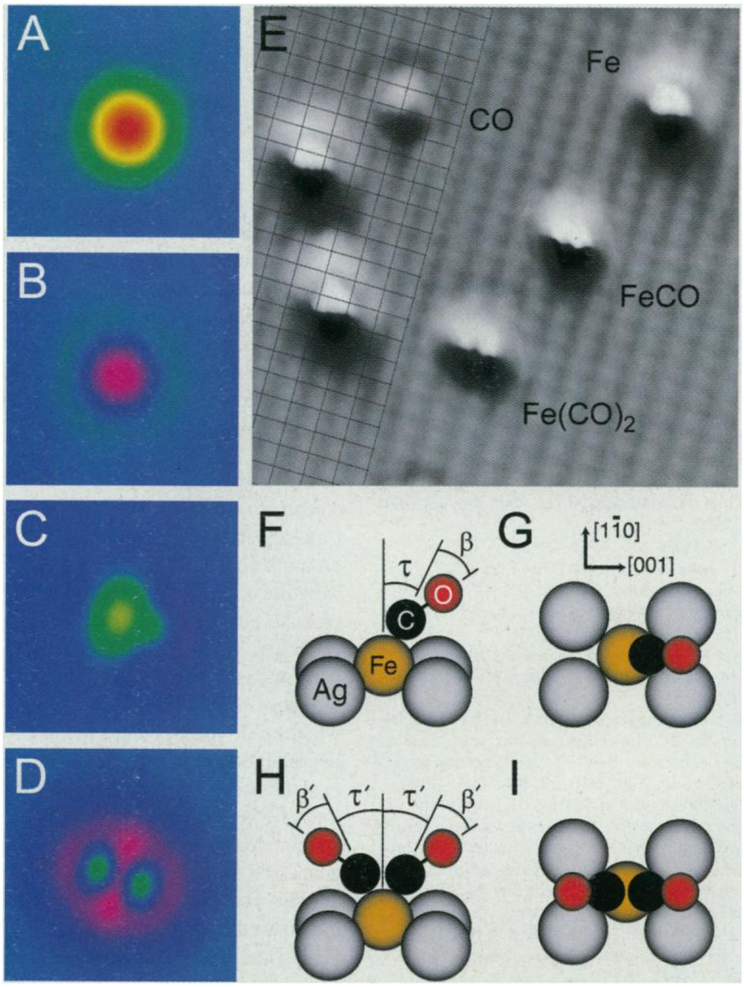

Fig. 4. 25 Å by 25 Å STM topographic images recorded at 70-mV bias and 0.1 nA without CO molecule attached to the tip for **(A)** Fe, **(B)** CO, **(C)** Fe(CO), and **(D)** Fe(CO)$_2$. **(E)** Atomically resolved STM topographic image recorded at 22-mV bias and 2.5-nA tunneling current with a CO molecule attached to the tip. The scanned area is the same as in Fig. 2D. All species, including CO, image as protrusions. The Fe(CO) image appears similar to that of Fe(CO)$_2$ because of frequent 180° flips (Fig. 2, C and D) during the scan with these tunneling parameters. In this image, it is not the tip height (z) that is displayed but its derivative (dz/dy), where y is the scan direction (from top to bottom). This has the effect of illuminating the scan area from the top side of the image and accentuating small corrugations. Therefore, each protrusion shows a bright illuminated side facing the top and a dark shadow facing the bottom. A grid is drawn through the Ag(110) surface atoms to guide the determination of the adsorption sites. **(F)** The side view and **(G)** top view of Fe(CO) show the CO to be tilted by angle τ and bent by angle β as suggested by the asymmetry in the image (C). The four-fold adsorption site is determined from (E). **(H)** The side view and **(I)** top view of Fe(CO)$_2$ show a similarly tilt-and-bent geometry with angles τ' and β' as implied by the images (D and E).

Spatially controlled bond formation has been realized with the STM. The fact that the CO ligand exhibits an inclined configuration in the Fe-Ag(110) system suggests that the observed geometry is due to the localized electronic properties of the Fe atom. In contrast, it would be interesting to determine if a single CO molecule would bond perpendicularly, without tilting or bending, with a different metal atom, such as Cu, on Ag(110) (*23*).

The binding of a diatomic molecule to an atom constitutes one of the simplest chemical transformations involving a molecule. By combining the present manipulation approach with other mechanisms such as "sliding" (*1*), "pulling," and "pushing" (*3, 4*), extension of spatially controlled bond formation to other atoms and molecules is envisioned. The ability to control step-by-step bond formation of adsorbed chemical species at the single-molecule level provides a real-space understanding and direct visualization of the nature of the chemical bond. An important function of STM-IETS lies in the confirmation and identification of the new bonds formed.

References and Notes

1. D. M. Eigler and E. K. Schweizer, *Nature* **344**, 524 (1990).
2. M. F. Crommie, C. P. Lutz, D. M. Eigler, *Science* **262**, 218 (1993).
3. L. Bartels, G. Meyer, K.-H. Rieder, *Phys. Rev. Lett.* **79**, 697 (1997).
4. J. K. Gimzewski and C. Joachim, *Science* **283**, 1683 (1999).
5. B. J. McIntyre, M. Salmeron, G. A. Somorjai, *Science* **265**, 1415 (1994).
6. B. C. Stipe, M. A. Rezaei, W. Ho, *Phys. Rev. Lett.* **81**, 1263 (1998).
7. ———, *Science* **280**, 1732 (1998).
8. ———, *Phys. Rev. Lett.* **82**, 1724 (1999).
9. B. C. Stipe *et al.*, *Phys. Rev. Lett.* **78**, 4410 (1997).
10. G. Dujardin, R. E. Walkup, Ph. Avouris, *Science* **255**, 1232 (1992).
11. The STM is a variation of the one described by B. C. Stipe, M. A. Rezaei, and W. Ho [*Rev. Sci. Instrum.* **70**, 137 (1999)].
12. Sample bias voltages greater than 2.4 V and tunneling currents of a few nanoamperes were used to transfer CO between the Cu(111) surface and the tip [L. Bartels *et al.*, *Phys. Rev. Lett.* **80**, 2004 (1998)].
13. The Fe(CO) can also be formed by pushing the CO with the tip toward the Fe atom at a sample bias of <70 mV and tunneling current of 10 nA. This process, however, is less controlled because the direction of motion of the CO is not predictable; the CO does not always follow the tip trajectory.
14. W. Erley, *J. Vac. Sci. Technol.* **18**, 472 (1981).
15. K. Tanaka, Y. Tachikawa, T. Tanaka, *Chem. Phys. Lett.* **281**, 285 (1997).
16. R. Fournier, *J. Chem. Phys.* **99**, 1801 (1993).
17. S. Hirota *et al.*, *J. Phys. Chem.* **98**, 6652 (1994).
18. On Ag(110), CO moves when it is scanned at 0.25 V and 1 nA, making it difficult to probe the C–O stretch by STM-IETS. However, the CO hindered rotation mode has been observed at 19 meV without causing the molecule to move. The C–O stretch is observed at 261 meV by high-resolution electron energy loss spectroscopy [R. A. Pelak and W. Ho, *Surf. Sci.* **321**, L233 (1994)].
19. The presence of the CO molecule on the tip is verified by changes in the STM topographical images (Fig. 2D versus Fig. 4E). Additional evidence is obtained by positioning the tip over a clean area on the Ag(110) surface and observing by STM-IETS two vibrational peaks: the hindered rotation at 19 meV and the C–O stretch at 267 meV for ${}^{12}C^{16}O$ and 253 meV for ${}^{13}C^{18}O$. These energies are close to those of CO on Ag(110) (*18*), suggesting that the tungsten tip is terminated with Ag because of physical contacts made with the surface during in situ tip conditioning.
20. O. González-Blanco and V. Branchadell, *J. Chem. Phys.* **110**, 778 (1999).
21. D. W. Moon, D. J. Dwyer, S. L. Bernasek, *Surf. Sci.* **163**, 215 (1985).
22. U. Burghaus and H. Conrad, *Surf. Sci.* **331-333**, 116 (1995).
23. A single CO molecule adsorbs vertically on an atop site through the carbon atom on both Cu(001) and Cu(110) surfaces as determined by STM-IETS [L. J. Lauhon and W. Ho, *Phys. Rev. B* **60**, R8525 (1999)].

24. Supported by the Department of Energy, Basic Energy Sciences grant DE-FG02-91ER14205.

10 August 1999; accepted 26 October 1999

Mechanical Rotation of the c Subunit Oligomer in ATP Synthase (F_0F_1): Direct Observation

Yoshihiro Sambongi,[1] Yuko Iko,[1] Mikio Tanabe,[1] Hiroshi Omote,[1]* Atsuko Iwamoto-Kihara,[2] Ikuo Ueda,[1] Toshio Yanagida,[3] Yoh Wada,[1] Masamitsu Futai[1]†

F_0F_1, found in mitochondria or bacterial membranes, synthesizes adenosine 5′-triphosphate (ATP) coupling with an electrochemical proton gradient and also reversibly hydrolyzes ATP to form the gradient. An actin filament connected to a c subunit oligomer of F_0 was able to rotate by using the energy of ATP hydrolysis. The rotary torque produced by the c subunit oligomer reached about 40 piconewton-nanometers, which is similar to that generated by the γ subunit in the F_1 motor. These results suggest that the γ and c subunits rotate together during ATP hydrolysis and synthesis. Thus, coupled rotation may be essential for energy coupling between proton transport through F_0 and ATP hydrolysis or synthesis in F_1.

The proton-transporting ATP synthase, F_0F_1, consists of a catalytic sector, F_1 or F_1–adenosine triphosphatase (ATPase) ($\alpha_3\beta_3\gamma_1\delta_1\epsilon_1$), and a proton pathway, F_0 ($a_1b_2c_{12}$) (*1, 2*). The crystal structure of the bovine $\alpha_3\beta_3\gamma$ complex indicates that the α and β subunits are arranged alternately around the NH_2- and COOH-terminal α helices of the γ subunit (*3*). The isolated F_1 hydrolyzes ATP, followed by γ subunit rotation, which is driven by conformational changes of the catalytic subunits (*4*). The γ subunit rotation in F_1 has been suggested by biochemical experiments (*5*) and has been observed directly as counterclockwise rotation of an actin filament connected to the γ subunit (*6, 7*).

The γ subunit rotation in F_1 should be transmitted to the membrane sector, F_0, in order to complete the ATP hydrolysis–dependent proton transport. The detailed underlying mechanism of the energy transmission between F_0 and the γ subunit remains unknown. If the c subunit oligomer rotates counterclockwise (the same direction as γ) in the membrane, the ATP hydrolysis–dependent γ subunit rotation could be connected mechanically to the F_0 sector. In this regard, c subunit rotation has been proposed (*2, 8*). However, to the best of our knowledge, this possibility of energy coupling has not been studied.

We designed several experimental systems to examine this possibility. The γ and ϵ complex is shown to be a rotor (*6–9*) and the α, β, δ, a, and b complex is proposed to be a stator in F_0F_1 (*8*). Therefore, we fixed F_1 α (or β) subunits on a glass surface to demonstrate the rotation of an actin filament connected to the F_0 c subunit, or conversely, the c subunits were fixed and the rotation of α or β was examined. ATP-dependent rotation was only successfully observed with the system described below (*10*). *Escherichia coli* F_0F_1 was immobilized on a coverslip through a His tag linked to the NH_2-terminus of each α subunit (Fig. 1). A c subunit Glu^2 was replaced by cysteine and then biotinylated to bind streptavidin and a fluorescently labeled actin filament. The γ subunit cysteine residues were replaced with alanine (*11*) in order to avoid direct binding of the actin filament to this subunit. Thus, cysteine is present only in the c subunit of the presumed rotor complex of the

---

[1] Division of Biological Sciences, Institute of Scientific and Industrial Research, Osaka University, CREST (Core Research for Evolutional Science and Technology) of Japan Science and Technology Corporation, Ibaraki, Osaka 567–0047, Japan. [2] Department of Biology, Graduate School of Arts and Sciences, University of Tokyo, Komaba, Tokyo 153–8902, Japan. [3] Department of Physiology, Osaka University Medical School, Suita, Osaka 565–0871, Japan.

*Present address: Department of Molecular Physiology and Biological Physics, University of Virginia, Charlottesville, VA 22906–0011, USA.

†To whom correspondence should be addressed. E-mail: m-futai@sanken.osaka-u.ac.jp

LINKED CITATIONS

You have printed the following article:

Single-Bond Formation and Characterization with a Scanning Tunneling Microscope
H. J. Lee; W. Ho
Science, New Series, Vol. 286, No. 5445. (Nov. 26, 1999), pp. 1719-1722.
Stable URL:
http://links.jstor.org/sici?sici=0036-8075%2819991126%293%3A286%3A5445%3C1719%3ASFACWA%3E2.0.CO%3B2-J

This article references the following linked citations:

References and Notes

[2] **Confinement of Electrons to Quantum Corrals on a Metal Surface**
M. F. Crommie; C. P. Lutz; D. M. Eigler
Science, New Series, Vol. 262, No. 5131. (Oct. 8, 1993), pp. 218-220.
Stable URL:
http://links.jstor.org/sici?sici=0036-8075%2819931008%293%3A262%3A5131%3C218%3ACOETQC%3E2.0.CO%3B2-H

[4] **Nanoscale Science of Single Molecules Using Local Probes**
James K. Gimzewski; Christian Joachim
Science, New Series, Vol. 283, No. 5408. (Mar. 12, 1999), pp. 1683-1688.
Stable URL:
http://links.jstor.org/sici?sici=0036-8075%2819990312%293%3A283%3A5408%3C1683%3ANSOSMU%3E2.0.CO%3B2-D

[5] **Nanocatalysis by the Tip of a Scanning Tunneling Microscope Operating Inside a Reactor Cell**
B. J. McIntyre; M. Salmeron; G. A. Somorjai
Science, New Series, Vol. 265, No. 5177. (Sep. 2, 1994), pp. 1415-1418.
Stable URL:
http://links.jstor.org/sici?sici=0036-8075%2819940902%293%3A265%3A5177%3C1415%3ANBTTOA%3E2.0.CO%3B2-Z

[7] **Single-Molecule Vibrational Spectroscopy and Microscopy**
B. C. Stipe; M. A. Rezaei; W. Ho
Science, New Series, Vol. 280, No. 5370. (Jun. 12, 1998), pp. 1732-1735.
Stable URL:
http://links.jstor.org/sici?sici=0036-8075%2819980612%293%3A280%3A5370%3C1732%3ASVSAM%3E2.0.CO%3B2-J

NOTE: *The reference numbering from the original has been maintained in this citation list.*

LINKED CITATIONS

- Page 2 of 2 -

[10] **Dissociation of Individual Molecules with Electrons from the Tip of a Scanning Tunneling Microscope**

G. Dujardin; R. E. Walkup; Ph. Avouris

Science, New Series, Vol. 255, No. 5049. (Mar. 6, 1992), pp. 1232-1235.

Stable URL:

http://links.jstor.org/sici?sici=0036-8075%2819920306%293%3A255%3A5049%3C1232%3ADOIMWE%3E2.0.CO%3B2-O

NOTE: *The reference numbering from the original has been maintained in this citation list.*